Crimson Publishers
Wings to the Research

Research Article

Tribological and Electrochemical Properties of TiO_2/DLC Coatings Produced on Ti-6Al-4V alloy by One-Step PEO

ISSN: 2578-0255

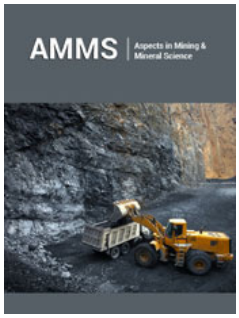

Sara Aghaie, Seyed Mohammad Hassan Pishbin and Mohsen Saremi*

School of Metallurgy and Materials Engineering, College of Engineering, University of Tehran, Iran

***Corresponding author:** Mohsen Saremi, School of Metallurgy and Materials Engineering, College of Engineering, University of Tehran, Tehran, Iran

Submission: April 07, 2025
Published: April 21, 2025

Volume 13 - Issue 3

How to cite this article: Sara Aghaie, Seyed Mohammad Hassan Pishbin and Mohsen Saremi*. Tribological and Electrochemical Properties of TiO_2/DLC Coatings Produced on Ti-6Al-4V alloy by One-Step PEO. Aspects Min Miner Sci. 13(3). AMMS. 000813. 2025.
DOI: 10.31031/AMMS.2025.13.000813

Abstract

Ti-6Al-4V alloy exhibits exceptional corrosion resistance in body fluid but is limited by its susceptibility to wear. Various methods were applied to improve its performance. Among them, PEO obtained more interest, especially when used as a composite with carbonaceous material. This study investigates the effect of adding different concentrations of Diamond-Like Carbon (DLC) nanoparticles during the one-step Plasma Electrolytic Oxidation (PEO) process on the microstructure, surface roughness, corrosion behavior, and wear resistance of the coating layer. Microstructural, morphological, and compositional analysis was achieved using SEM, XRD, and Raman spectroscopy techniques. The results showed that DLC nanoparticles were successfully integrated into PEO coatings, improving the corrosion and wear resistance. The highest corrosion resistance and the lowest wear rate were obtained in the sample coatings with 2g/L of DLC nanoparticles, in which the wear rate was significantly lower than Ti-6Al-4V coated with and without DLC nanoparticles, respectively.

Keywords: Coating; Plasma electrolytic oxidation; Ti-6Al-4V alloy; Diamond-like carbon; Corrosion; Wear

Introduction

Ti-6Al-4V alloy has been widely used as an implant material due to its biocompatibility, good immunity to corrosion, and high strength-to-weight ratio [1-3]. However, along with the aforementioned benefits, it also has some weaknesses related to wear characteristics that can curtail its performance [4-6]. A thin layer of titanium oxide is naturally formed on the surface of titanium alloys, which provides an appropriate biological response and reduces harmful ions released from its surface. Nevertheless, the prolonged use of titanium implants results in abrasion and mechanical loads that destroy the protective oxide. This eventually leaves the substrate exposed to corrosive or abrasive environments in the body [7,8]. Hence, the useful life of the implant is reduced by increasing the probability of allergic reactions and implant loosening caused by the release of toxic ions or wear particles into surrounding implant tissues [9]. To address this problem, forming an appropriate protective coating using the PEO process can be an effective surface treatment procedure. As the surface is treated with the PEO technique, a high number of micro-discharges appear as a result of dielectric breakdown. During the PEO process, two layers, a dense layer adjacent to the substrate and a porous layer on the top are formed. The porosity is due to the movement of the molten metal caused by localized melting in the discharge channels. Apart from the electrical parameters, the electrolyte composition also influences the structure and properties of the produced coating layer [10]. For example, KOH and NaOH increase electrolytic conductivity, silicate-based electrolytes create thicker and rougher coatings with lower adhesion, and phosphate-based

electrolytes exhibit low roughness and high adhesion. Aluminate-based electrolytes can enhance wear resistance due to the formation of hard phases like Al_2O_3 and Al_2TiO_5, while their effectiveness is reduced by poor adhesion to the substrate [10,11]. Several strategies have been used to enhance the PEO coating performance, where the oxidized surface can be further sealed or hybrid coated with functional materials [12-15]. Chemical substances were also added to an electrolyte prior to PEO coating to improve the Ti-6Al-4V alloy performance [16-22]. Among most other materials, carbon derivatives offer unique characteristics to the PEO layer [23,24]. Diamond-Like Carbon (DLC) is a metastable phase consisting of crystalline and amorphous carbon, which predominantly exhibits good biocompatibility, chemical resistance, and a low coefficient of friction [25-27].

However, its functionality is compromised when mechanical properties are mismatched and there is insufficient adhesion between the DLC film and the metal surface [28,29]. Many approaches have been employed to improve the performance of DLC coating, including incorporating intermediate layers prior to DLC deposition [7,30,31], doping DLC with elements like fluorine [32], and creation of a ceramic base by PEO to apply DLC film [33-35]. Among these strategies, there is a lack of research on a composite coating of TiO_2/DLC solely through PEO treatment. Therefore, this study investigates the microstructure, corrosion, and tribological properties of DLC-containing oxide coating on Ti-6Al-4V alloy using a one-step PEO process at different concentrations of DLC-dispersed phosphate-base electrolyte.

Material and Methods

Ti-6Al-4V alloy sheet was cut into square plates with dimensions of 30mm×30mm×2mm. The chemical composition of Ti-6Al-4V alloy according to the supplier's specifications is given in Table 1. To prepare the specimens for PEO treatment, one side of all the samples was polished with abrasive SiC paper up to 2000 grits to remove the natural oxide layer, and the other side was attached to the wire and then sealed with mounting material. The samples were ultrasonically cleaned in a mixture of deionized water and alcohol for 10 minutes and thoroughly dried under warm air. The TiO_2/DLC composite coating was applied in one-step PEO with parameters of applied voltage in the range of 300-400V, process time of 5 minutes, frequency of 1000Hz, and duty cycle of 40%, as shown in Figure 1. Dynamic light scattering (DLS, NanoDS) with scattering angle of 30° and solvent temperature of 25 °C was used to measure the average size and volume distribution of DLC particles. As shown in Figure 2, the volume average diameter of DLC particles was 66.9nm. To prepare an electrolyte bath, Na_3PO_4 (10g/L) and NaOH (5g/L) with various concentrations of DLC from 0 to 0.5, 1, 2, and 3g/L (the samples are designated S0, S1, S2, S3, and S4, respectively) were added in 1000mL distilled water. The electrolyte solution was sonicated prior to PEO and placed on a magnetic stirrer along the process to ensure that the solution was perfectly homogeneous and prevented temperature gradients. The mentioned samples were served as anodes, and a stainless-steel cooling coil was used as cathodes in addition to maintaining the temperature of the electrolyte bath below 30 °C during the procedure.

Table 1: Chemical composition of Ti-6Al-4V.

Ti	Al	V	O	Fe	C	N	H
balanced	5.99	3.95	0.17	0.14	0.011	0.009	0.004

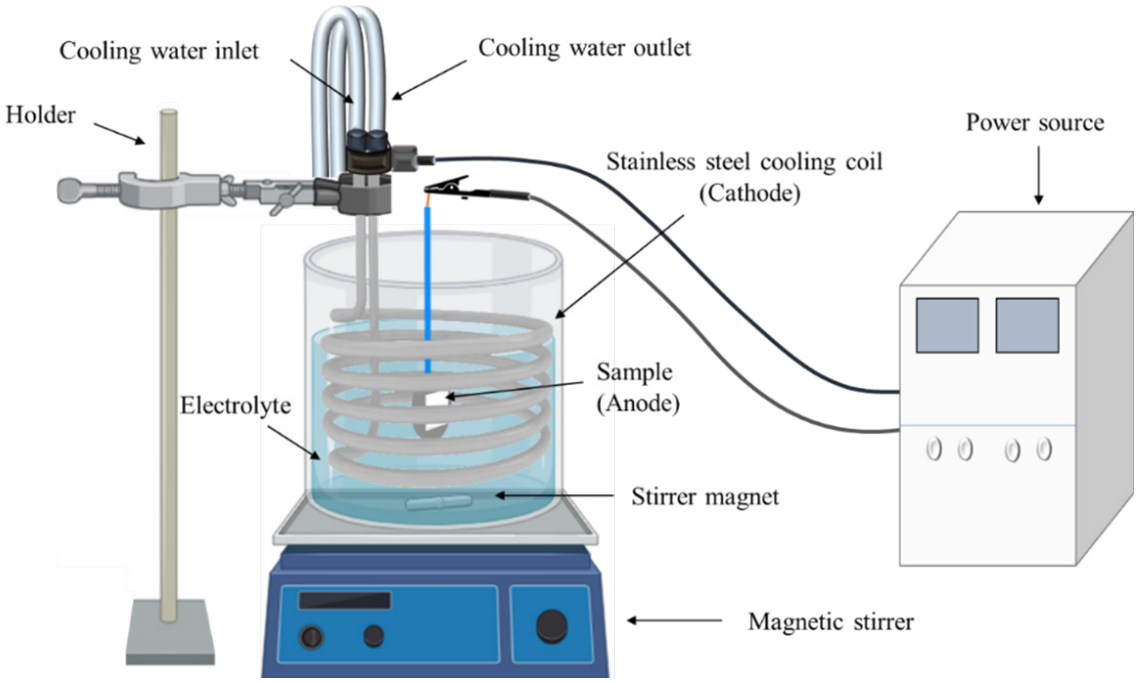

Figure 1: Schematic representation of experimental setup used in the PEO process.

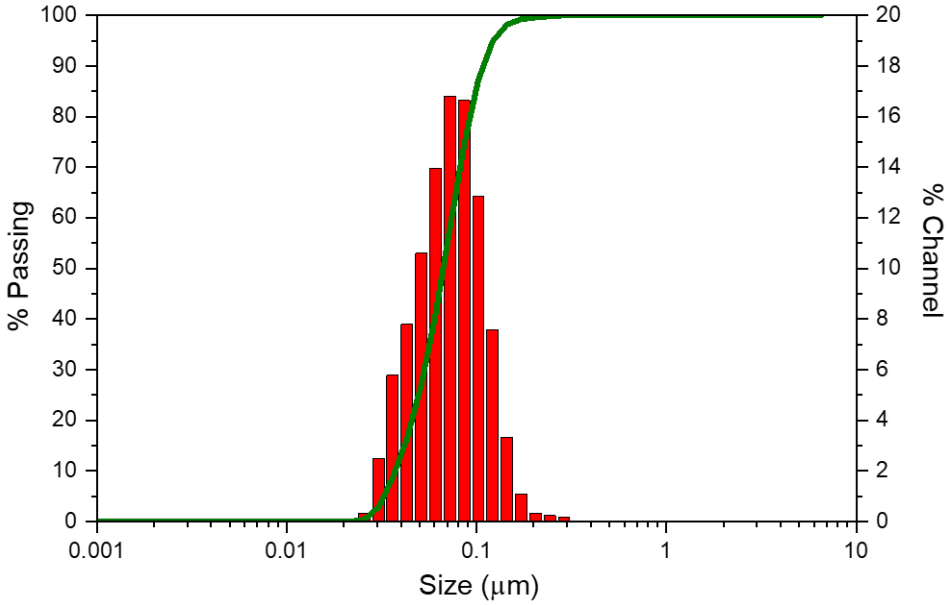

Figure 2: Particle size distribution of DLC measured by DLS.

Surface characterization

A Tescan Mira3 Scanning Electron Microscope (SEM) coupled with Energy Dispersive X-Ray (EDX) was utilized to observe the surface morphology and cross-sectional analysis. Average pore size and porosity percentage were estimated using Image J. Phase composition of the produced coatings was also analyzed by Phillips X' Pert X-Ray Diffraction Method (XRD) using Cu Kα radiation (λ=1.54Å, 40kV, 30mA). The graphitization degree of DLC/PEO samples was analyzed by Raman spectroscopy (Takram P50C0R10, Teksan) with an Ar laser beam at 532nm wavelength. The surface roughness parameters of the samples were evaluated by a surface roughness measuring machine (Hommelwerke T8000 Stylus Profilometer) with a test speed of 0.15mm/s.

Corrosion tests

The Tafel Polarization corrosion test was performed using Solarton model 1286 to obtain a polarization curve with a scan rate of 5mV/s. Buffer Phosphate Saline (PBS) solution at pH=7.4 and 37 °C was used as the electrolyte, a Saturated Calomel Electrode (SCE) as a reference, a Pt wire as the counter electrode, and the samples as working electrodes. The surface area of the working electrode was set as 1.0cm^2. The samples were immersed in the solution for about 30 minutes prior to corrosion tests to achieve stable open circuit potential. The corrosion potential (E_{corr}) and corrosion current density (i_{corr}), etc., were fitted by the Tafel extrapolation method.

Friction tests

Wear tests were performed using a reciprocating tribometer at room temperature and a humidity level of 50%. A ball with a diameter of 3mm made of Al_2O_3 was used as the abrasive material. The tests were performed under a normal load of 2N, linear sliding speed of 1.2cm/s, frequency of 2Hz, wear length of 6mm, and time of 40 minutes. The Coefficient of Friction (COF) was automatically and continuously recorded during the test as a function of the sliding distance. After the wear test, the roughness test was used to check the depth and width of the wear, and the SEM was used to check the structure of the wear path and reveal the wear mechanism.

Result and Discussion

Characterization of PEO coatings

SEM images of the coating surface produced in phosphate-based electrolytes containing different DLC additives are given in Figure 3. Initial PEO coating (Figure 3a) exhibited a porous structure with fine pores and micro cracks, attributed to electrochemical reactions and thermal stresses generated during the coating process. The average size of these pores was approximately 1.12μm, and the overall porosity of the coating was 9.5%. The coating morphology was significantly changed by adding DLC nanoparticles to the electrolyte. The average pore size for sample S1 increased to 2.42μm, while, in S2, S3, and S4, it decreased to 0.76μm, 0.97μm, and 1.32μm. There are numerous rounded interconnected pores at the top surface of sample S1 (Figure 3b). Sample S2 exhibited flat pores with non-uniform distribution surrounded by smooth regions (Figure 3c). At the highest DLC concentration of 3g/L, there was a poor dispersion of DLS in the electrolyte, leading to the formation of DLC aggregates. This reduced uniformity in the DLC distribution within the solution directly compromises the quality of the resulting coating (Figure 3e_1). Figure 3 (e_2, e_3) illustrates that DLC nanoparticles have contributed to the formation of a ceramic coating by adsorption on the surface and into micro pores (Figure 3e_2). Hence, they integrate into the coating layer as it grows, forming a unique volcanic rock-like structure (Figure 3e_3).

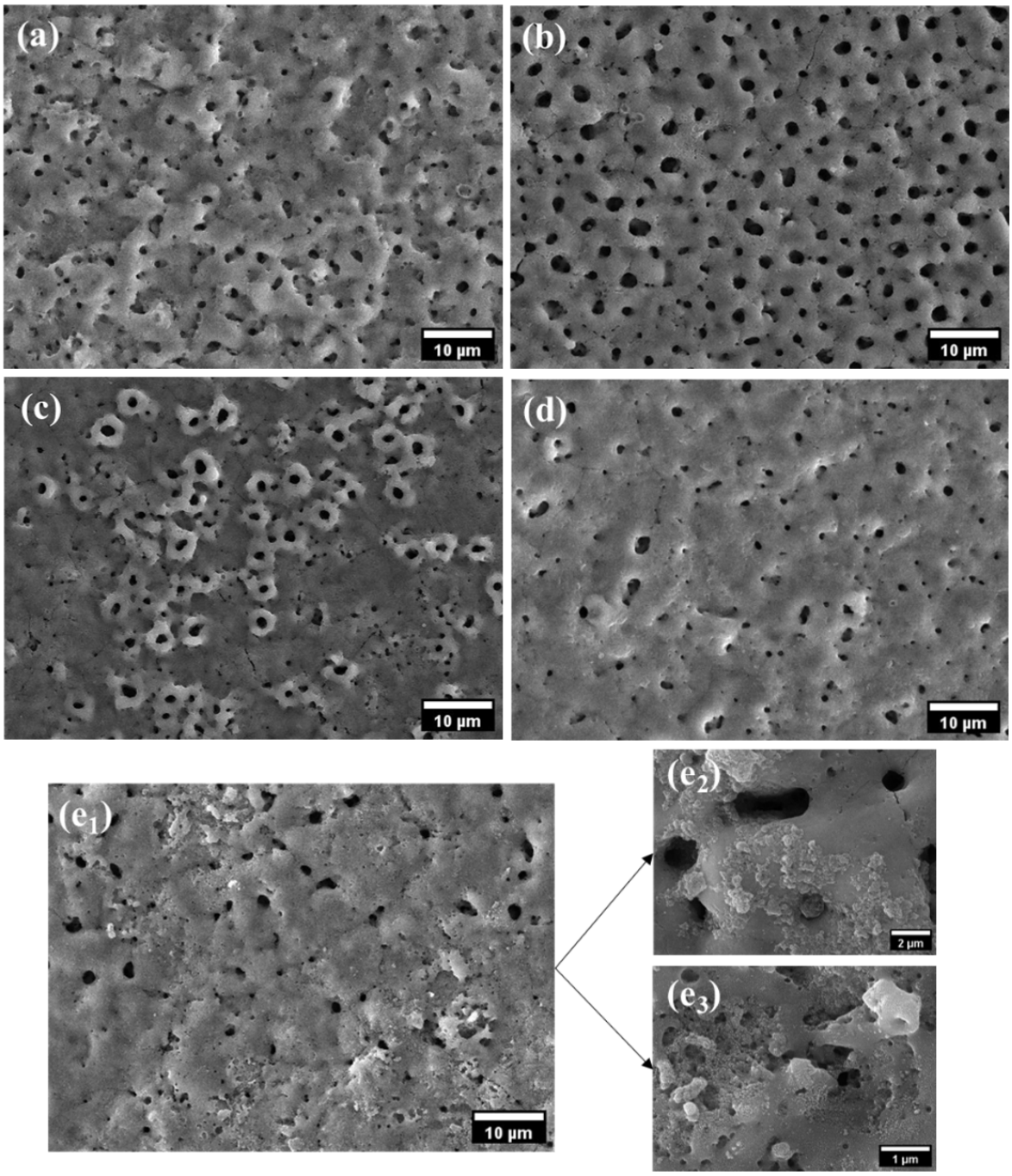

Figure 3: SEM micrographs of PEO coatings obtained in the electrolytes with different DLC concentrations. (a) S0, (b) S1, (c) S2, (d) S3, and (e_1, e_2, e_3) S4.

The cross-section images of PEO coating samples showed a porous outer layer and a compact barrier layer located next to the substrate (Figure 4). The oxide coatings are bonded well to the titanium base metal with no visible crack but have some cavities due to the formation of gas bubbles during the breakdown process. The formation of a fragile and porous shell in S4 may occur due to the aggregation or interference of nanoparticles with the oxide growth process, resulting in a less compact and weaker coating. Thicker coatings with a denser structure tend to have better overall quality especially superior tribological performance [36]. As the concentration of nanoparticles increases, the overall surface roughness of the coating increases. The average roughness for samples S0, S1, S2, S3, and S4 was 0.53µm, 0.52µm, 0.29µm, 0.65µm, and 0.73µm, respectively. These observations indicate that the incorporation of nanoparticles into the PEO coating leads to a rougher surface texture that might be caused by aggregation of nanoparticles or uneven deposition on the surface, which can create a new set of peaks and valleys and increase the roughness for samples S4.

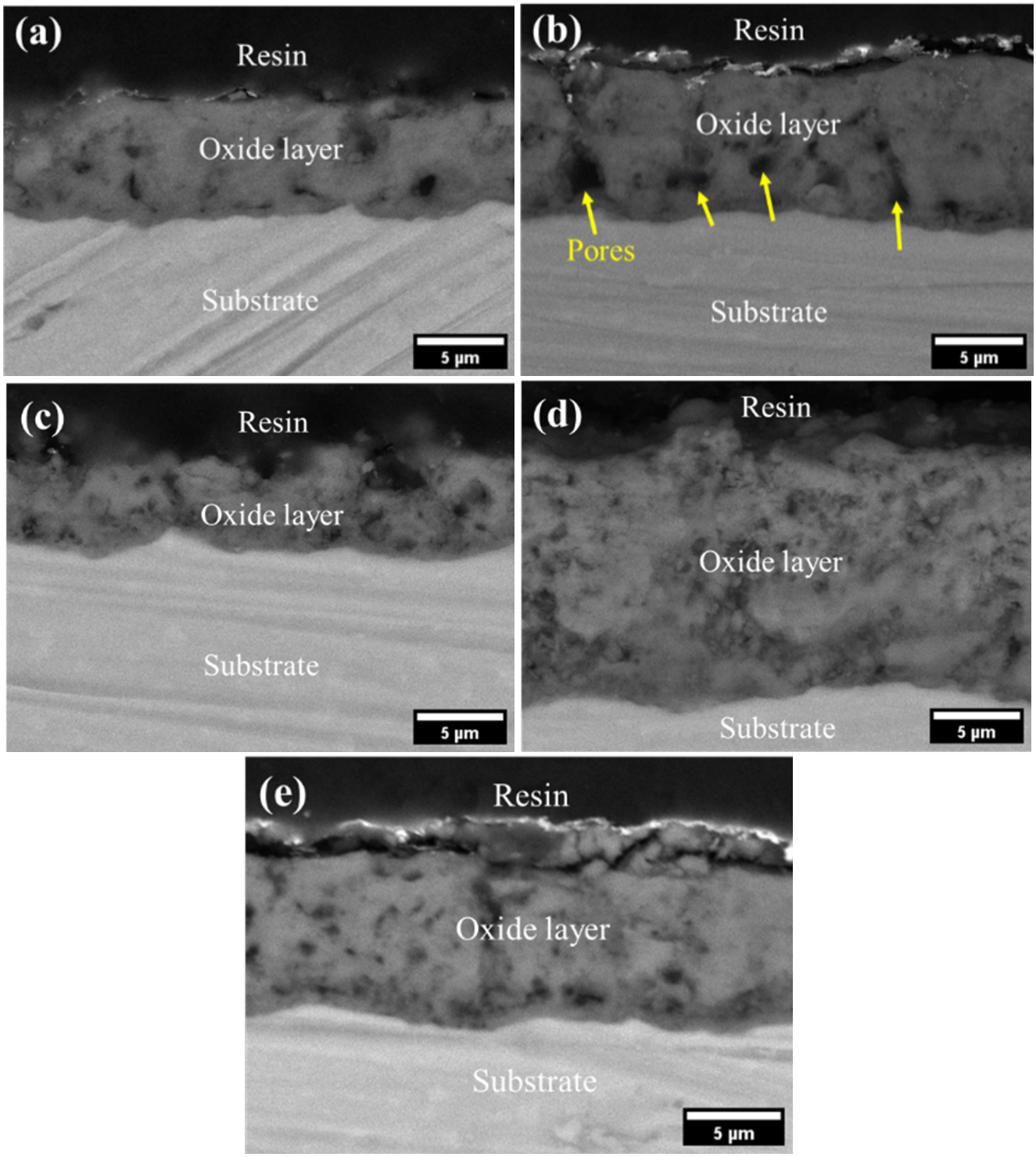

Figure 4: Cross-sectional SEM images of PEO coatings obtained in the electrolytes with different DLC concentrations. (a) S0, (b) S1, (c) S2, (d) S3, and (e) S4.

The spectra obtained from XRD test for the samples with nanocomposite coating compared to the S0 sample are presented in Figure 5. The discharge has enough energy to melt the coating material, which forms a highly crystalline oxide coating when the discharges stopped, and the material is quenched [33]. Titanium oxides, including anatase and rutile, can be seen in all samples with different intensities. The appearance of the Ti peak of the substrate is due to the penetration of X-rays in the porous structure of the thin coating layer. The intensity of the titanium peak in the S2 sample with the lowest thickness of the oxide layer is higher than the other samples, and it is the lowest value for the S3 sample. By increasing the concentration of nanoparticles in the electrolyte, it can be seen that the intensity of the peaks associated with the rutile phase has increased significantly. The reason for this can be

explained by the increase in conductivity of the electrolyte with the increase in the concentration of nanoparticles, which can lead to a localized temperature rise, which facilitates the conversion of anatase to rutile [16].

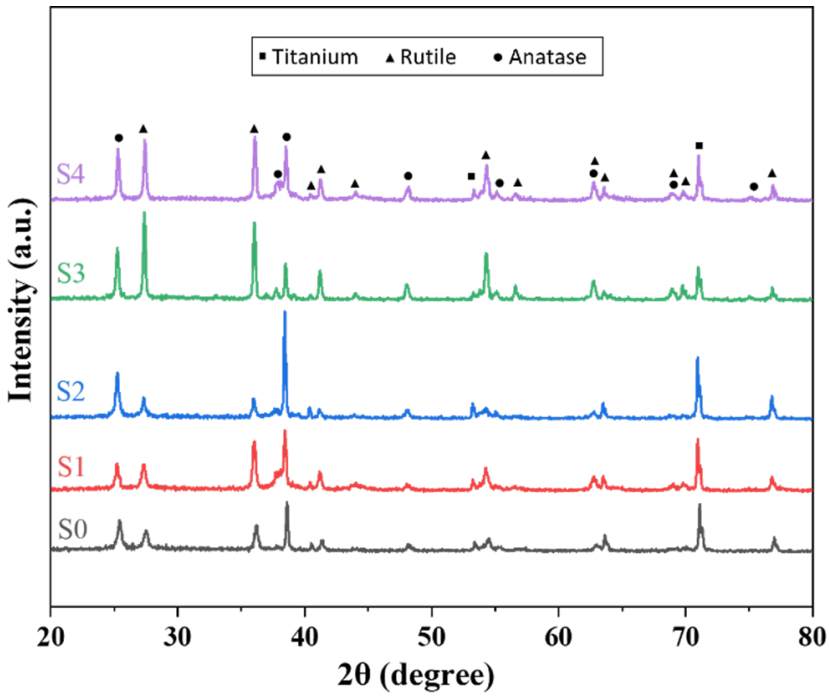

Figure 5: XRD patterns of PEO coatings with different amounts of DLC nanoparticles.

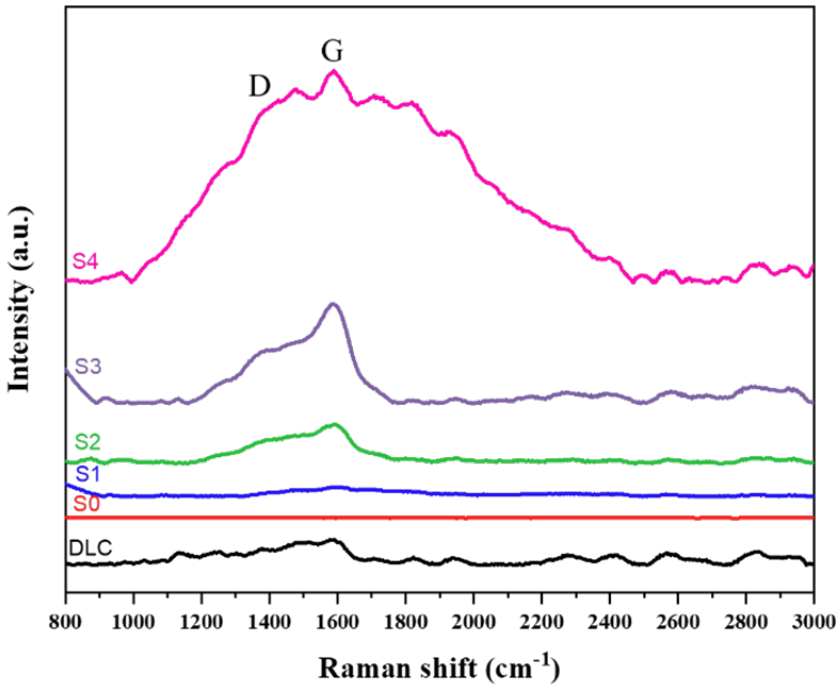

Figure 6: Raman spectrum of PEO Coated Samples Compared to DLC spectrum.

Raman spectroscopy of samples with and without DLC nanoparticles is shown in Figure 6. A reference DLC Raman spectrum, obtained from DLC nanoparticles, is provided for comparative analysis of coating peak positions. It can be seen that there are several peaks in the Raman shift range of 1000-3000cm^{-1} for the spectrum of the composite coatings, in good agreement with the D peak (disordered graphite-like) at 1350-1450cm^{-1} and G peak (carbon bond of graphite) at 1500-1600cm^{-1}. By measuring the intensities of the G and D peaks in the Raman spectrum and calculating the I_D/I_G ratio, we can determine the sp^2/sp^3 ratio in

the DLC film [34,37]. The I_D/I_G ratio for S1, S2, S3, and S4 coating samples was about 0.51, 0.68, 0.61, and 0.77, respectively. These observations further prove the incorporation of nanoparticles into the coating during the PEO process. Notably, agglomeration and adsorption of DLC nanoparticles were not widely observed on the surface of the samples. However, due to the presence of D and G peaks in Raman spectroscopy of these samples, it can be deduced that DLC nanoparticles were successfully incorporated in the ceramic matrix during PEO process, and TiO_2/DLC composite is created on the Ti-6Al-4V surface in the DLC dispersed phosphate-based electrolyte. With the increase in the concentration of DLC nanoparticles, the D and G bonds intensified, indicating improvement in the incorporation of DLC into the coating layer. The increased peak width observed in the Raman spectrum of sample S4 indicates a more disordered carbon structure, potentially resulting from higher substrate/electrolyte temperatures during the PEO process.

Potentiodynamic polarization analysis

Figure 7 shows the Tafel polarization curves of bare and coated samples in PBS solutions at 37 °C. Determined electrochemical variables are given in Table 2. The introduction of oxide coatings employing the PEO technique enhanced the corrosion resistance of Ti-6Al-4V biomedical alloy, resulting in a positive shift of E_{corr} and polarization curves. Sample S3 showed the highest corrosion potential (0.242V vs. SCE) and the smallest corrosion current value (2.40×10^{-8}A/cm^2), which can be related to the formation of a thicker oxide layer that acts as a barrier against a corrosive environment. However, the polarization curve for S4 shows a shift towards more negative potentials compared to S3, which is due to the formation of a weak layer, as evidenced by cross-sectional analysis, and an increase in the size of the pores in this sample. Due to the role of pores in allowing corrosive body fluids to reach the base material, there is a positive correlation between pore size and corrosion resistance [33]. Furthermore, the increased corrosion susceptibility of the S4 coated substrate can be attributed to the aggregation of nanoparticles on the surface or interference with the oxide growth process at this high concentration and results in relatively high electrical conductivity of these coatings that facilitates the transfer of electrons from the S4 sample (anode). This behavior indicates a deterioration of the corrosion resistance of sample S4, which contradicts the general trend observed in samples S1 to S3, which means the coating integrity deteriorates.

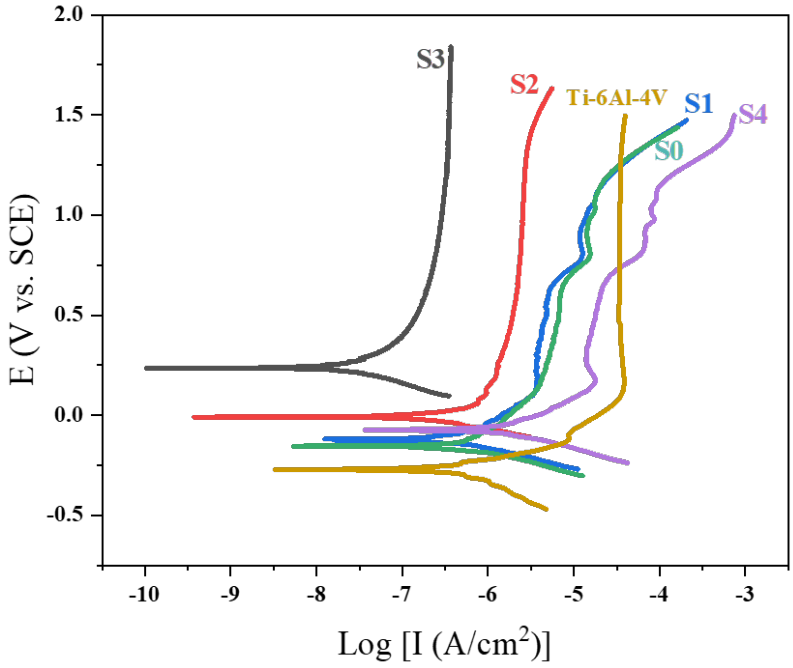

Figure 7: Polarization plots of Ti-6Al-4V, S0, S1, S2, S3, and S4 samples in PBS solution.

Table 2: Polarization data of Ti-6Al-4V, S0, S1, S2, S3, and S4 in PBS solution.

Samples	E_{Corr} (V vs. SCE)	I_{Corr} (A/cm^2)	βa (mV)	βc (mV)	Rp (kΩ.cm^2)
Ti-6Al-4V	-0.272	5.16×10^{-7}	112.76	204.65	61.20
S0	-0.154	5.82×10^{-7}	322.64	111.76	61.87
S1	-0.124	4.48×10^{-7}	261.2	106.66	73.46
S2	-0.007	1.60×10^{-7}	79.6	78.51	107.13
S3	0.242	2.40×10^{-8}	216.48	130.45	1469.03
S4	-0.075	1.87×10^{-6}	227.79	123.87	18.66

Wear behavior

The SEM images and wear test results after the linear reciprocating wear test of the samples are shown in Figure 8 & 9, and Table 3. The S0 sample has very high friction when sliding against an alumina ball. The TiO_2 coating, although harder than uncoated Ti-6Al-4V, exhibits abrasive wear and detachment, resulting in a high friction coefficient and wear rate. In contrast, the TiO_2/DLC composite coatings have low friction throughout the test, suggesting that it reduces friction better than the uncoated Ti-6Al-4V alloy or the TiO_2 coating alone. This improvement is likely due to DLC nanoparticles in the composite coating, which act as a self-lubricant during the sliding process. Wear scar analysis indicated that samples S2 and S3 exhibited significantly less wear volumes than the others, while sample Ti-6Al-4V demonstrated the most extensive wear volume. Abrasive grooves are observed parallel to the alumina ball sliding direction on the wear scar morphology of uncoated Ti-6Al-4V alloy (Figure 9a). The addition of DLC coincided with a reduction in coating destruction. The composite coatings exhibited delamination in specific regions, forming numerous craters on the worn surface (Figure 9). This delamination can be attributed to the coating's susceptibility to brittle fracture under cyclic stress conditions encountered during the sliding test. The pore-rich microstructure of the coating is still observed on the wear surface of sample S1. It can be said that the frictional pressure compressed the ridges into the pores and absorbed the incoming force (Figure 9c). A similar result was observed in a previous investigation [38]. Sample S3 demonstrates exceptional tribological performance, exhibiting a lower COF and wear rate than the TiO_2 coating and substrate. This is evident in the wear track's minimal depth and width, as shown in Table 3. This composite coating effectively reduces friction and protects the Ti-6Al-4V alloy from severe wear. By comparing the wear depth values and the coatings' thickness (Figure 4), it can be said that the wear was formed only in the oxide layer region, and the substrate was not exposed. No evidence of the PEO coatings detaching from the substrate after testing indicated strong adhesion between the layers. The literature has also reported that friction accelerates the sp^3 to sp^2 conversion and thus creates a graphite-like transfer film on the DLC surface, which participates in surface lubrication [35]. As was evident in the cross-sectional images, in the S4 sample, despite the increased presence of lubricant nanoparticles on the surface of the coating, depending on the interaction between the nanoparticles and the growing oxide layer, weak interfaces were created in the upper layer of the coating structure, which it potentially reduces overall cohesion results in higher wear volume compared to other samples containing nanoparticles. Also, the surface roughness of sample S4 was reported to be higher than that of other samples, which caused more abrasive oxide to be transferred from the material to the wear path.

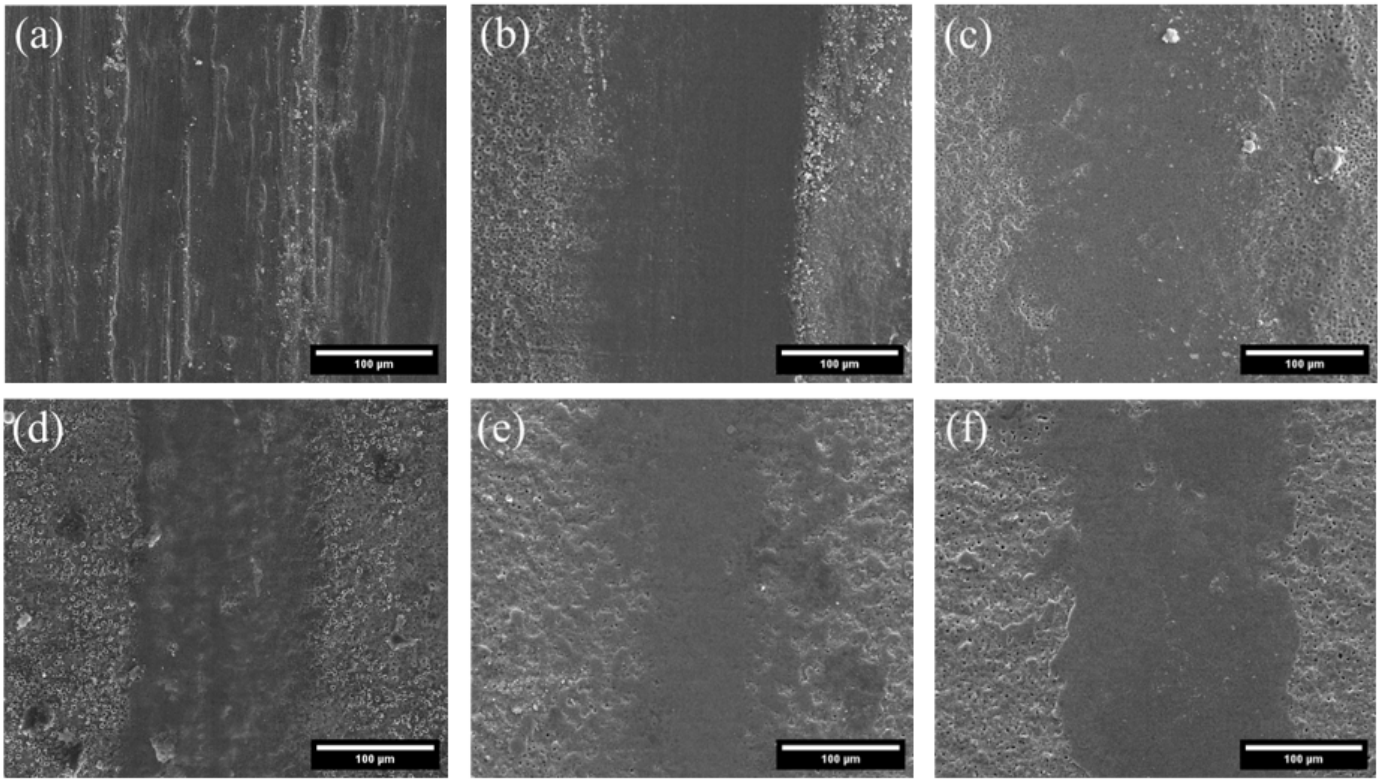

Figure 8: Wear track images of untreated and coated samples. (a) Ti-6Al-4V, (b) S0, (c) S1, (d) S2, (e) S3, and (f) S4.

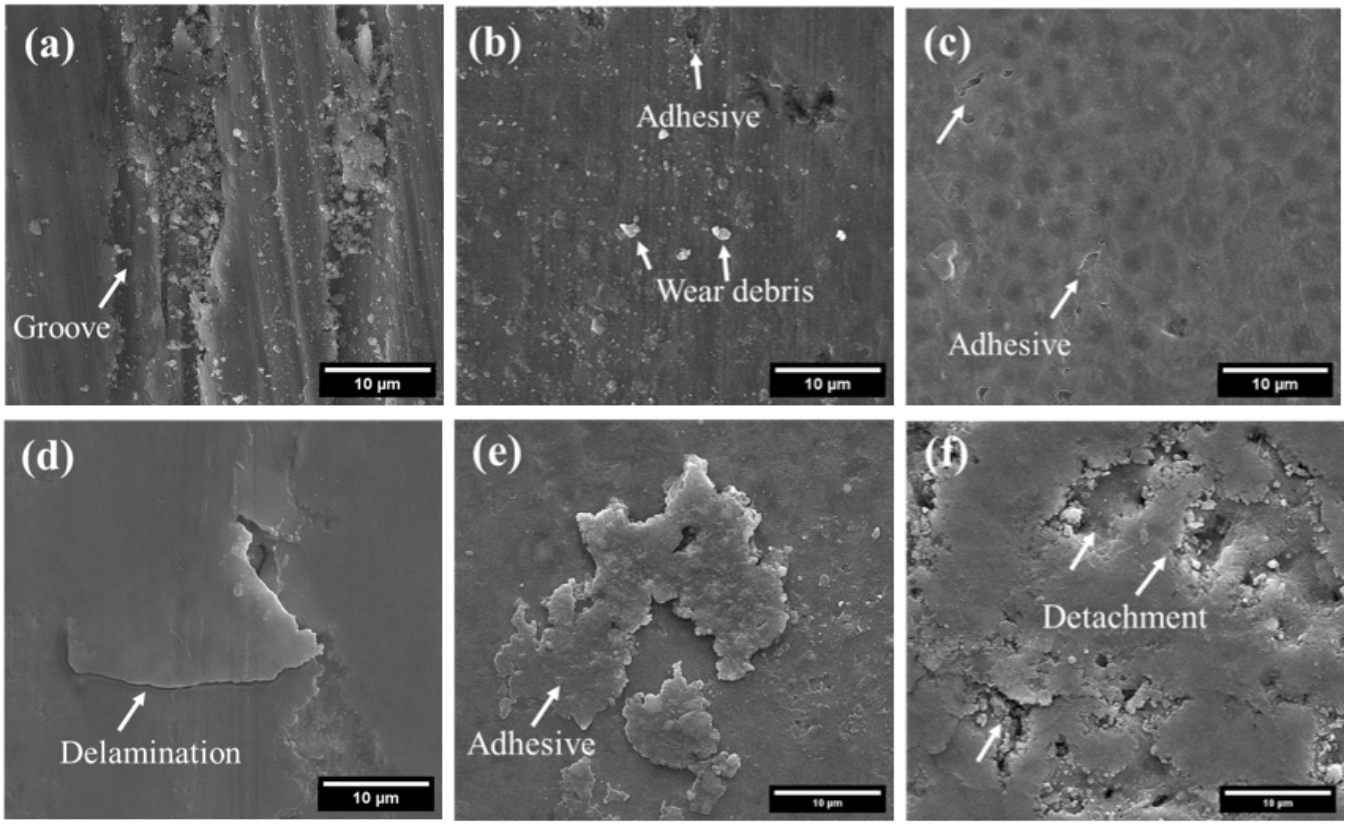

Figure 9: Wear track images of untreated and coated samples. (a) Ti-6Al-4V, (b) S0, (c) S1, (d) S2, (e) S3, and (f) S4.

Table 3: Wear test results of uncoated and PEO-coated samples.

Samples	Average COF	Wear Depth (µm)	Wear Width (µm)	Wear Volume 10^{-12} (m^3)	Wear Rate 10^{-15} (m^3/N.m)
Ti-6Al-4V	0.1336	8.861	523.799	13.241	1.103
S0	0.3316	7.288	195.261	5.755	0.481
S1	0.1300	2.567	182.591	3.334	0.277
S2	0.0829	2.981	158.413	0.994	0.083
S3	0.0886	0.911	115.666	0.285	0.024
S4	0.086	3.851	196.760	5.212	0.434

Conclusion

In this study, the effect of the PEO process and the addition of DLC nanoparticles on the properties of the coatings created on the Ti-6Al-4V alloy was investigated. The effect of DLC addition on the structure, morphology, corrosion, and wear of the coatings has been evaluated. The following conclusions are obtained from this investigation:

a. The presence of DLC nanoparticles in the coating changes the shape and size of the pores. The oxide coatings adhere firmly to the substrate without any detachments in all samples.

b. In all coated samples, anatase and rutile titanium oxide phases were detected. The Raman spectrum shows that DLC nanoparticles are integrated into the structure of PEO coatings. Increasing the concentration of nanoparticles increased the intensity of the peaks related to G and D.

c. Potentiodynamic polarization curves showed the beneficial effect of nanoparticles on the corrosion resistance of PEO coatings on Ti-6Al-4V alloy up to a concentration of 2g/L. However, excessive concentration of nanoparticles led to adverse effects.

d. The highest wear resistance was achieved by the coating produced in phosphate base solution and 2g/L of DLC nanoparticles, showing a much smaller wear volume.

e. The addition of DLC nanoparticles, in optimum concentration, improved the adhesion, corrosion resistance, and wear resistance of oxides formed on Ti-6Al-4V by PEO.

Acknowledgement

Many thanks to Dr. Changiz Dehghanian for the assistance with coatings' deposition.

References

1. Bocchetta P, Chen LY, Tardelli JDC, Dos Reis AC, Almeraya-Calderón F, et al. (2021) Passive layers and corrosion resistance of biomedical Ti-6Al-4V and β-Ti alloys. Coatings 11(5): 487.
2. Zhang K, Zhang W, Yang Y, Sun X, Men B, et al. (2024) Enhanced hydrophobic properties, wear and corrosion resistance of plasma electrolyte oxidation coatings on AZ31B magnesium alloys with addition of TiO_2 nanoparticles. Ceramics International 50(24): 52941-52956.
3. Kei Lung CY (2017) Surface coatings of titanium and zirconia. Advanced Material Science 2:
4. Nisar SS, Choe HC (2024) TiO_2 coatings doped with MoS_2 nanoparticles using plasma electrolytic oxidation on Ti-6Al-4V alloy: Application for enhanced and functional bio-implant surface. Journal of Materials Research and Technology 33: 2035-2056.
5. Cooke K, Alhubaida A (2022) Microstructural response and wear behaviour of Ti-6Al-4V impregnated with $Ni/Al_2O_3 + TiO_2$ nanostructured coating using an electric arc. Scientific Reports 12:
6. Sun X, Zhou J, Xu K, Wu W, Xu L, et al. (2023) Effects of different factors on the friction and wear mechanical properties of titanium alloy materials with cortical bones at near service conditions. PLoS ONE 18:
7. Kang S, Lim HP, Lee K (2015) Effects of TiCN interlayer on bonding characteristics and mechanical properties of DLC-coated Ti-6Al-4V ELI alloy. International Journal of Refractory Metals and Hard Materials 53: 13-16.
8. Quinn J, McFadden R, Chan CW, Carson L (2020) Titanium for orthopedic applications: An overview of surface modification to improve biocompatibility and prevent bacterial biofilm formation. IScience 23(11): 101745.
9. Kheder W, Al Kawas S, Khalaf K, Samsudin AR (2021) Impact of tribocorrosion and titanium particles release on dental implant complications-A narrative review. Japanese Dental Science Review 57: 182-189.
10. Aliofkhazraei M, Macdonald DD, Matykina E, Parfenov EV, Egorkin VS, et al. (2021) Review of plasma electrolytic oxidation of titanium substrates: Mechanism, properties, applications and limitations. Applied Surface Science Advances 5: 100121.
11. Pesode P, Barve S (2021) Surface modification of titanium and titanium alloy by plasma electrolytic oxidation process for biomedical applications: A review. Materials Today: Proceedings 46: 594-602.
12. Ji R, Wang S, Zou Y, Chen G, Wang Y, et al. (2023) One-step fabrication of amorphous/ITO-CNTs coating by plasma electrolytic oxidation with particle addition for excellent wear resistance. Applied Surface Science 640: 158274.
13. Li T, Li L, Qi J, Chen F (2020) Corrosion protection of Ti6Al4V by a composite coating with a plasma electrolytic oxidation layer and sol-gel layer filled with graphene oxide. Progress in Organic Coatings 144: 105632.
14. Yu S, Liu Y, Zhang R, Ge X, Li J, et al. (2023) Lubrication and anti-wear behavior of duplex annealed nanodiamonds/PEO coating on Ti6Al4V: Functional mechanism of structural transformation. Surface and Coatings Technology 461: 129426.
15. Zhang Y, Wang Q, Ye R, Ramachandran CS (2022) Plasma electrolytic oxidation of cold spray kinetically metallized CNT-Al coating on AZ91-Mg alloy: Evaluation of mechanical and surficial characteristics. Journal of Alloys and Compounds 892: 162094.
16. Guo Y, Xu L, Luan J, Wan Y, Li R (2022) Effect of carbon nanotubes additive on tribocorrosion performance of micro-arc oxidized coatings on Ti6Al4V alloy. Surfaces and Interfaces 28: 101626.
17. Guo Z, Yang Z, Chen Y, Li H, Zhao Q, et al. (2022) One-step plasma electrolytic oxidation with graphene oxide for ultra-low porosity corrosion-resistant TiO_2 coatings. Applied Surface Science 594: 153477.
18. Li X, Dong C, Zhao Q, Pang Y, Cheng F, et al. (2018) Characterization of microstructure and wear resistance of PEO coatings containing various microparticles on Ti6Al4V alloy. Journal of Materials Engineering and Performance 27: 1642-1653.
19. Mu M, Zhou X, Xiao Q, Liang J, Huo X (2012) Preparation and tribological properties of self-lubricating TiO_2/graphite composite coating on Ti6Al4V alloy. Applied Surface Science 258(22): 8570-8576.
20. Nadimi M, Dehghanian C (2021) Incorporation of ZnO-ZrO_2 nanoparticles into TiO_2 coatings obtained by PEO on Ti–6Al–4V substrate and evaluation of its corrosion behavior, microstructural and antibacterial effects exposed to SBF solution. Ceramics International 47(23): 33413-33425.
21. Yang C, Cui S, Wu Z, Zhu J, Huang J, et al. (2021) High efficient co-doping in plasma electrolytic oxidation to obtain long-term self-lubrication on Ti6Al4V. Tribology International 160: 107018.
22. Yu JM, Choe HC (2019) Morphology changes and bone formation on PEO-treated Ti-6Al-4V alloy in electrolyte containing Ca, P, Sr, and Si ions. Applied Surface Science 477: 121-130.
23. Babaei K, Fattah-alhosseini A, Molaei M (2020) The effects of carbon-based additives on corrosion and wear properties of Plasma electrolytic oxidation (PEO) coatings applied on aluminum and its alloys: A review. Surfaces and Interfaces 21: 100677.
24. Fattah-alhosseini A, Molaei M, Nouri M, Babaei K (2021) Review of the role of graphene and its derivatives in enhancing the performance of plasma electrolytic oxidation coatings on titanium and its alloys. Applied Surface Science Advances 6: 100140.
25. Mochalin VN, Shenderova O, Ho D, Gogotsi Y (2012) The properties and applications of nanodiamonds. Nature Nanotechnology 7: 11-23.
26. Hirata Y, Kato T, Choi J (2015) DLC coating on a trench-shaped target by bipolar PBII. International Journal of Refractory Metals and Hard Materials 49: 392-399.
27. Tyagi A, Walia RS, Murtaza Q, Pandey SM, Tyagi PK, et al. (2019) A critical review of diamond like carbon coating for wear resistance applications. International Journal of Refractory Metals and Hard Materials 78: 107-122.
28. Sharifahmadian O, Pakseresht A, Amirtharaj Mosas KK, Galusek D (2023) Doping effects on the tribological performance of diamond-like carbon coatings: A review. Journal of Materials Research and Technology 27: 7748-7765.
29. Wang K, Zhou H, Zhang K, Liu X, Feng X, et al. (2021) Effects of Ti interlayer on adhesion property of DLC films: A first principle study. Diamond and Related Materials 111: 108188.
30. Buyanovskii IA, Samusenko VD, Levchenko VA (2020) Antifriction properties of a diamond-like coating and titanium nitride in model lubricating media. Journal of Machinery Manufacture and Reliability 49: 389-394.
31. Wu Y, Shi B, Liu Y, Wang L, Gao J, et al. (2022) Design of Ta gradient layer to improve adhesion strength between Cu substrate and DLC film. Vacuum 203: 111221.
32. Wang J, Ma J, Huang W, Wang L, He H, et al. (2017) The investigation of the structures and tribological properties of F-DLC coatings deposited on Ti-6Al-4V alloys. Surface and Coatings Technology 316: 22-29.
33. Molak RM, Topolski K, Spychalski M, Dulińska-Molak I, Morończyk B, et al. (2019) Functional properties of the novel hybrid coatings combined of the oxide and DLC layer as a protective coating for AZ91E magnesium alloy. Surface and Coatings Technology 380: 125040.

34. Shahin N, Shamanian M, Kharaziha M (2022) Electrochemical behavior of the double-layer diamond-like carbon/plasma electrolytic oxidation on AZ31 alloy: A comparison of different PEO interlayers. Diamond and Related Materials 130: 109405.

35. Sukuroglu EE, Totik Y, Arslan E, Efeoglu I (2015) Analysis of tribo-corrosion properties of MAO/DLC coatings using a duplex process on Ti6Al4V alloys. Journal of Bio- and Tribo-Corrosion 1.

36. Durdu S, Usta M (2014) The tribological properties of bioceramic coatings produced on Ti6Al4V alloy by plasma electrolytic oxidation. Ceramics International 40(2): 3627-3635.

37. Cui XJ, Ning CM, Zhang GA, Shang LL, Zhong LP, et al. (2021) Properties of polydimethylsiloxane hydrophobic modified duplex microarc oxidation/diamond-like carbon coatings on AZ31B Mg alloy. Journal of Magnesium and Alloys 9(4): 1285-1296.

38. Karimi M, Jafari Eskandari M, Araghchi M (2024) Fabrication and characterization of graphene oxide/zirconium dioxide coatings produced by plasma electrolytic oxidation of Zr–1%Nb alloys. Results in Surfaces and Interfaces 14: 100205.